Chemical Engineering Journal 148 (2009) 139–144

Contents lists available at ScienceDirect

Chemical Engineering Journal

journal homepage: www.elsevier.com/locate/cej

Modeling of residence time distribution: Application to a three-phase inverse fluidized bed based on a Mellin transform

L. Montastruc[a,*], J.P. Brienne[b], I. Nikov[a]

[a] Polytech'Lille, Département IAAL, ProBioGEM, Université des Sciences et Technologies de Lille, Cité Scientifique, Avenue Paul Langevin, 59655 Villeneuve d'Ascq, France
[b] Polytech'Lille, Département IAAL, LAGIS UMR CNRS 8146, Université des Sciences et Technologies de Lille, Cité Scientifique, Avenue Paul Langevin, 59655 Villeneuve d'Ascq, France

ARTICLE INFO

Article history:
Received 12 December 2007
Received in revised form 18 August 2008
Accepted 19 August 2008

Keywords:
RTD
Inverse fluidized bed
Mellin transform

ABSTRACT

The study is focused on modeling of gas and liquid residence time distribution in an aerated liquid system of an inverse fluidized bed bioreactor. Two opposite strategies are currently available: the use of powerful complex computational fluid dynamics (CFD) simulation and the phenomenological semi-empirical models. In this work, a specific methodology is proposed, as follows: the reactor is modeled as a reactor network containing a combination of zones with basic ideal flow patterns such as perfect mixed flow (PMF) and plug flow (PF). The approach is based on a Mellin-modification of the Laplace transformation over the relevant equations. The method allows zero-time solutions for identification analysis. The study shows that the increase of the gas flowrate leads to higher mixing intensity of the gas phase. Decreasing the gas velocity, the inverse fluidized bed tends to perform as a plug flow reactor. The liquid phase performs closer to disperse plug flow.

1. Introduction

The inverse fluidized bed is realized with solid particles having density lower than the continuous phase liquid which flows downward in the reactor downward flow of continuous liquid phase. In three-phase inverse fluidized beds (TPIFB), the gas phase is introduced counter currently to the liquid phase. This type of reactor is gaining popularity in biotechnology and various industrial applications such as ethanol production and wastewater treatment. The TPIFB shows several advantages, such as high mass transfer, rate lower solids attrition of the coated microorganisms, efficient control of the biofilm thickness and ease of refluidization [1–3].

It is important to note that the reactor operates with three phases under anaerobic as well as aerobic conditions. Some works have been carried out to characterize the hydrodynamic conditions in the liquid phase [4,5]. These studies show that the dispersed plug flow model can be reasonably used to describe the phase mixing in the reactor. Recent results show that the gas velocity influences the biofilm compositions [6]. The control of the hydrodynamic conditions in a biofilm reactor should make possible to obtain a resistant and active biofilm. However, when the liquid velocity increases, the abrasion phenomenon increases too. Therefore, it is important to find the appropriate liquid flowrate, in order to achieve fluidization.

The present study is focused on modeling of gas and liquid residence time distribution. Two opposite strategies are available now: the powerful but complex computational fluid dynamics (CFD) simulation and the simple phenomenological structural models. The CFD in gas–liquid contactors requires description at some complex phenomena in particular bubbles break up or coalescence [7]. In view of this, new approach to modeling the liquid and gas phase behavior in a three-phase inverse fluidized bed is proposed. The method has some advantages, such as easy to use and giving quick answers. Due to the use of the Mellin transformation, it is not necessary to optimize the parameter with a MINLP optimization method but just with the quadratic programming optimization method. The objective is to propose a methodology based on the tracer RTD technique extended by a new system identification approach using Mellin transformation.

2. Experimental

The configuration of the inverse fluidized bed reactor applied was based on the pilot scale unit presented in our previous work [2,8]. Two reactors were used in this study. For the liquid phase study, the diameter was 0.102 m and the height 1.3 m whereas for the gas phase study, the diameter was 0.05 m and the height 1.1 m. Thus, the volume was 10.62 and 2.15 l, respectively.

The production of the carrier was based on a procedure similar to that one proposed by Nikov et al. [2], which included surface treatment of expanded polystyrene beads with polymethyl-metacrylate

* Corresponding author.
E-mail address: Ludovic.Montastruc@polytech-lille.fr (L. Montastruc).

1385-8947/$ – see front matter © 2008 Elsevier B.V. All rights reserved.
doi:10.1016/j.cej.2008.08.035

and powdered activated carbon. Solid particle density was between 350 and 650 kg/m^3. Temperature was maintained at $20 \pm 1\,^{\circ}C$.

A Dirac pulse was selected to characterize the liquid RTD. As a means of detection, a blue dye tracer and a LED and photocell were used. A tracer dye concentration of 10 ml per liter of the solution gave sufficient output intensity (i.e. voltage drop as measured by the voltmeter used) to minimize the measurement error. This choice was driven by the photocell technology. Besides, the Dirac pulse gives more information than the step function.

The gas RTD curves were obtained following step change disturbances in the gas feed (nitrogen into air) [9]. Oxygen concentration was analyzed continuously by SERVOMEX 4100 analyzer equipped with a paramagnetic detector. All the experiments were repeated for reproducibility.

The Dirac pulse input is more difficult to be realized than the step but in the case of pulse input the experimental residence time distribution was more informative. The difference between the step input and the Dirac pulse is fundamental: the step input is the Dirac pulse integral. So, the step brings less information than the Dirac pulse but the experimental points obtained by the step are the surest. In this case, if the pulse is chosen the mathematical model must be perfectly fitted to the experimental data.

3. Mathematical model

For solving the problem, different approaches are possible: the simplest way is to use an axial plug flow model [4], another way is to use a reactor network model [10,11]. The model was formulated as a network of discrete ideal flow components: plug flow reactor (PFR) and perfect mixing reactor (PMR) combined. Each branch was characterized by specific parameters (flowrate branch, PFR volume, PMR in serial number (n) and the PMR volume). The n and N values were integers and determined the model superstructure. The N values represented the branch number. The model adjustment was carried out by comparison of the simulated model response to a stimulus, and the experiments' response. The following flow chart represented the model network (Fig. 1):

Generally, to solve this kind of a problem, a superstructure has to be used to represent as adequately as possible the reactor. In this case, it would be necessary to use a mixed integer no linear programming program. Consequently, the solving strategy was based on a master program (e.g. is a stochastic method to reduce the number of iterations) that proposes network structures to a slave program for the optimization of the continuous variables (such as flowrates and volumes) corresponding to each cell arrangement (such as by quadratic programming (QP) or sequential quadratic programming method (SQP)). Yet, this strategy requires a test procedure for detecting the infeasibility of some structures proposed by the stochastic method.

In order to determine the fluid RTD, a specific approach based on a mathematical model describing the concentration time-course in the Laplace domain was used.

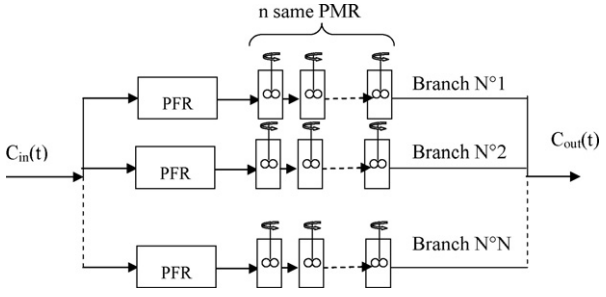

Fig. 1. Model network representation.

The equation describing the PFR is

$$c_{out}(t) = c_{in}(t - \tau_{PFR}) \tag{1}$$

In the Laplace domain, the Eq. (1) is

$$C_{out}(p) = C_{in} \exp(-p\tau_{PFR}) \tag{2}$$

With p the Laplace variable.

For the PMR, the specific equation is

$$c_{out}(t) = c_{in}(t) * \frac{1}{\tau_{PMR}} \exp\left(-\frac{t}{\tau_{PMR}}\right) \tag{3}$$

With $*$ representing the convolution product characterizes by:

$$c_{out}(t) = c_{in}(t) * h(t) = \int_0^t c_{in}(t-u)h(u)\,du \tag{4}$$

In the Laplace domain, the Eq. (3) is

$$C_{out}(p) = C_{in}(p)\left(\frac{1}{p + (1/\tau_{PMR})}\right)\frac{1}{\tau_{PMR}} \tag{5}$$

The equation for one branch composed by PFR and n PMR in the Laplace domain is as follows:

$$C_{out}(p) = C_{in}(p)\left(\left(\frac{1}{p + (1/\tau_{PMR})}\right)\frac{1}{\tau_{PMR}}\right)^n \exp(-\tau_{PFR}p) \tag{6}$$

So for the global system in Fig. 1, the model in the Laplace domain is

$$C_{out}(p) = C_{in}(p)\sum_{i=1}^{N}\frac{\lambda_k a_i^n}{(p + a_i)^n} \exp(-T_i p) \tag{7}$$

With $a_i = (1/\tau_{PMR})$, $T_i = \tau_{PFR}$, λ_i represents the reduced partial flowrate and $n \in N^+$.

The model included the transfer function with $k_i = \lambda_i a_i^n$:

$$H(p) = \frac{C_{out}(p)}{C_{in}(p)} = \sum_{i=1}^{N}\frac{k e^{-Ti\,p}}{(p + a_i)^{n\,i}} \tag{8}$$

So, $T_i\lambda_i Q_g = (T_i k_i / a_i^{n_i})Q_g$ represents the plug flow reactor volume n_i is equal to the number of perfect stirred reactor in serial and $(Q_g\lambda_i/a_i) = (k_i Q_g / a_i^{n_i} a_i)$ represents the perfect stirred reactor volume. In Eq. (8), n_i value is a continuous value.

The use of Mellin transformation allowed determination of the parameter values by a SQP method because all parameters are continuous. If this transformation was not used, it would be necessary to use a MINLP optimization method. In this case, it would be more difficult to determine the parameter values. The Eq. (8) was written using the Mellin transformation.

The equivalence between the Mellin transformation makes it possible to obtain the relations connecting the parameters of the two equations $H_r(p)$ and $H(p)$ (see Appendix 1).

$$H_r(p) = \frac{k\,e^{-Tp}}{(a+p)^n} \equiv H(p) = \frac{k'\,e^{-T'p}}{(a'+p)^{n'}} \tag{9}$$

With $T = T' + T''$.

Theses parameters are characterized by

$$\frac{k'}{a'^{n'}} = \frac{k}{a^n} \tag{10}$$

$$\frac{n'}{a'} = \frac{n}{a} + T'' \tag{11}$$

$$\frac{n'}{a'^2} = \frac{n}{a^2} \tag{12}$$

By imposing n with as condition $0 < n < n'$, the parameters are defined by

$$\frac{1}{a} = \frac{1}{a'}\sqrt{\frac{n'}{n}} \tag{13}$$

$$T'' = \frac{n'}{a'} - \frac{n}{a} \tag{14}$$

when $n = 0$, $T'' = (n'/a')$.

In order to determine the number of the series that represent the network, the second derivative of the response curve was determined numerically in the case of an experimental step. For the experimental Dirac pulse, it is necessary to derivate just one time the experimental curve because the step represented the Dirac pulse integral. Thus, the slope changes corresponding to the separate effects (phenomena) could be evaluated. Correspondingly, the slope changes represented the series of the relevant model network. Prior to the analysis, the output was filtered and the high frequency noise was eliminated.

A spectral decomposition is used (see Eq. (15)):

$$X(lf_o) = \frac{1}{T_0}\int_0^{T_0} s(t)\exp(-2\pi\ i l f_o t) \tag{15}$$

With $s(t)$ periodic signal with T_0 period, l is the ray number $f_o = (1/T_0)$ and $i^2 = -1$.

Using the spectral decomposition, low filter is applied for rebuilding the initial signal without the noise (see Eq. (16)):

$$s(t) = \sum_{n=0}^{L} X(lf_o)\exp(2\pi\, i l f_0 t) \tag{16}$$

The aim to use the filter was to determine the minimal number of branch in the superstructure with keep the maximum physical phenomena without noise.

Parameters $H_r(p)$ corresponding to the separate network branches can be determined by optimization using the least squares criterion applied to the difference between the output $C_{out}(t)$ and the experimental data (see Eq. (17)). Regarding the operation regimes subject to validation, the following constraints have to be considered:

$$J = \min \sum (c_{exp} - c_{out})^2 \tag{17}$$

The sum of flowrate is equal to 1.

$$\sum \frac{k_i}{a_i^n} = 1 \tag{18}$$

The sum of the volume is lower than the total reactor volume.

$$\sum T_i \frac{k_i}{a_i^{n_i}} Q_g + \sum n_i \left[\frac{k_i}{a_i^{n_i}} \frac{Q_g}{a_i}\right] \le V_{reactor} \tag{19}$$

The number of the perfect serials reactor transformation in integer value is described in the following paragraph. To conform reality, the n_i value is transformed into an integer value n_i'. Fig. 2 summarizes the modeling methodology.

4. Results and discussion

4.1. Example model evaluation of the liquid phase residence time distribution of TPIFB

Firstly, a spectral decomposition was realized according to Eq. (15). The signal was obtained during 64 s with a sampling period equal to 1s. The $X(lf_o)$ modulus was obtain for l value comprised between 0 and 32 using Eq. (15) in discrete-time. In Fig. 3, several

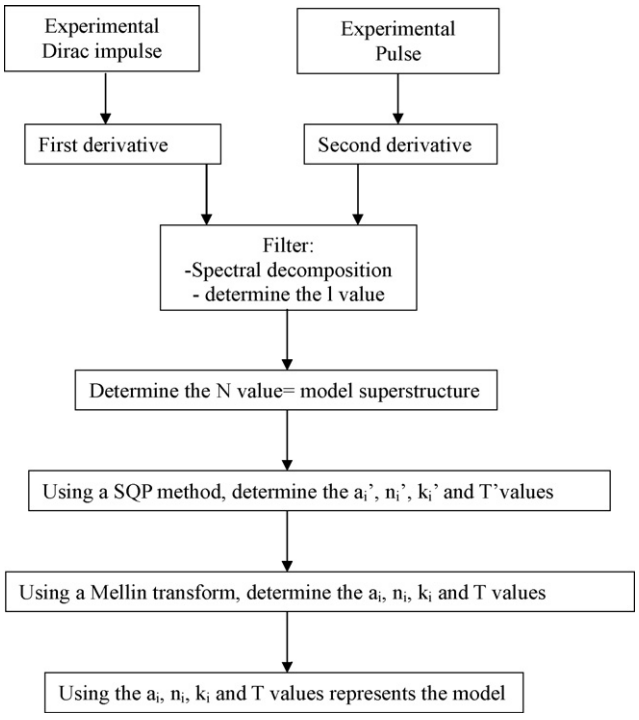

Fig. 2. Modeling methodology.

minimum were observed according different values l. The l selected values was 7, 11, 16 and 20. For each l value, the first derivative of the signal was filtered and the slope change number was determined, this number corresponds to the N branch number in the model (8) (N value was an integer values).

To study the filter influence according to the l values (id. cut frequency), the N branch number was determined in Table 1. When the cut frequency was high, the N value was also elevated. Whereas with a low cut frequency, the oscillatory phenomena in the high frequency was equal to the phenomena in the low frequency (See Fig. 4).

The real parameters obtained by QP optimization are shown in Table 2. According to the method described (Eqs. (10)–(14)), the serial reactor number should be changed to an integer value (see

Table 1
Filter frequency influence on the N branch number

l values	7	11	15	20
Cut frequency (Hz)	0.11	0.17	0.25	0.31
N branch number	5	7	15	19

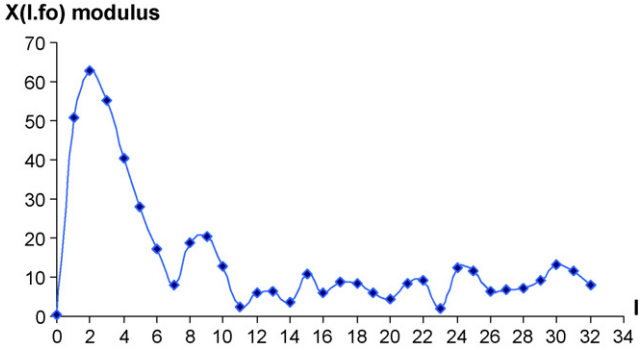

Fig. 3. Spectral decomposition.

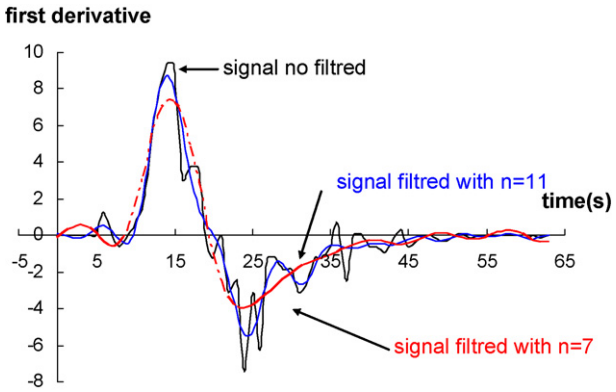

Fig. 4. First derivative of experimental points.

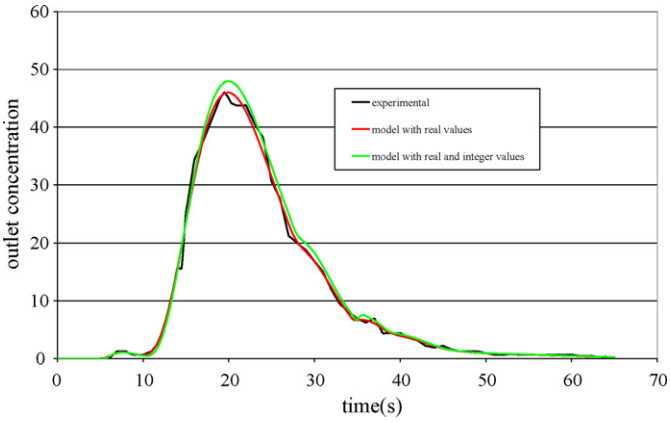

Fig. 5. Example of results: gas velocity (0.2 cm/s) and liquid velocity (6.7 cm/s).

Table 2
Real parameters

$T_i(s)$	$a'_i(1/s)$	n'_i	k'_i
4.99	1.1	3.97	9.20×10^{-3}
8.87	0.42	5.68	6.54×10^{-3}
26.97	0.73	3.95	9.95×10^{-3}
34.42	0.96	2.99	11.42×10^{-3}
35.46	0.92	3.98	6.03×10^{-3}
37.48	0.61	3.98	2.77×10^{-3}
44.05	0.24	3.14	0.17×10^{-3}

Table 3). The outlet concentration according time was represented in Fig. 5. The first peak occurring before 10 is due to a by pass in the inverse fluidized bed. Normally, the aim in the reactor is to reduce this phenomenon, in this experiments this phenomena represented less than 1% of the total phenomena. So it is interesting to modeling this peak in order to analyze the influence on the RTD. The second peak represented 90% in the RTD. The liquid mixing may be represented in our system by the axial dispersed plug-flow regime. In fact in Fig. 5, the modeling curve is the same as the experimental curve.

In Table 4, the various parameters are transformed in physical values (e.g. perfect mixed reactor volume, plug flow volume and stagnant volume. The result obtained show that the liquid phase behavior is near to a dispersed plug flow regime. The portion of stagnant volume in the reactor was high in comparison of the plug flow volume. It can be seen from this table that the axial dispersion increases according to the liquid velocity because the portion of the stagnant and the perfect mixed volume increases in comparison the plug flow behavior. The axial dispersion coefficient increases with the liquid velocity what is typical for the classical liquid/solid fluidized bed [1,12].

Table 3
Real and integer parameters

$T_i(s)$	$a_i(1/s)$	n_i	k_i	Gain $= \frac{k_i}{a_i^n}$
5.46	0.96	3.00	5.51	0.0063
9.71	0.39	5.00	8.58	0.9027
27.67	0.64	3.00	8.88	0.0345
34.99	0.79	2.00	7.95	0.0129
36.03	0.80	3.00	4.28	0.0084
38.34	0.53	3.00	2.94	0.0198
44.34	0.23	3.00	0.20	0.0153

Table 4
Volume (%) of each reactor type for a gas velocity (0.2 cm/s)

Liquid velocity (cm/s)	Plug flow	Perfect mixed reactor	Stagnant volume
4	80.5	2.1	17.4
6.7	63.5	5.0	31.5

4.2. Example model evaluation of gas phase residence time distribution in TPIFB

During this experiment, a step input of tracer was used for different reasons. Firstly, it was difficult to insure that a Dirac pulse was homogenous in the totality of the column section in particular in the gas phase. Moreover, the oxygen analyser could not detect this variation when the Dirac pulse (air/N_2) was used. In Fig. 7, the outlet concentration with a Dirac pulse was modeling. The behavior of the liquid flow in the reactor is affected by the gas flowrate.

Four gas flowrates were analyzed. To model the experiments points, we used the same methodology described in the previous paragraph. A typical example of the response curves to step change disturbances in the gas feed is shown in Fig. 6. The reduced outlet concentration was referred to the inlet concentration.

The various experiments were corresponded to different gas velocities. When gas velocity increased, the residence time decreased. Firstly, when the gas flowrate increased in coalescence regime the gas hold-up increased also. Essadki et al. [12] developed some correlations in coalescence regime or break-up regime. Moreover, the size of the bubble was linked with the gas hold-up. So, when the gas flowrate increased, the gas hold-up increased and the bubble size increased, and the bubble velocity increased so the residence time decreased.

The comparisons between experimental and model results are illustrated in Fig. 6.

Table 5
Volume (%) of each reactor type for different gas velocity

U_g (cm/s)	Plug flow reactor volume (%)	Perfect mixed reactor volume (%)	Stagnant volume (%)
2.12	17.7	82.3	0.0
1.41	43.7	54.4	1.9
0.7	44.6	52.5	2.9
0.35	55.8	44.2	0.0

Table 6
Parameters value obtained after optimization method

$T'_i(s)$	$a'_i(1/s)$	n'_i	$\frac{k'_i}{a'^{n'}_i} = \frac{k_i}{a_i{}^{n}}$	a_i	n_i	$T_i(s)$
U_g = 0.35 cm/s						
1.18E+02	1.53E−01	6.62E+00	2.01E−01	1.46E−01	6.00E+00	1.20E+02
1.68E+02	1.05E−02	1.43E+00	6.74E−01	8.76E−03	1.00E+00	1.91E+02
2.15E+02	9.51E−03	3.37E+00	1.25E−01	8.97E−03	3.00E+00	2.35E+02
U_g = 0.7 cm/s						
5.94E+01	1.90E−02	1.40E+00	8.77E−01	1.61E−02	1.00E+00	7.07E+01
1.43E+02	1.25E−02	1.95E+00	1.20E−01	8.91E−03	1.00E+00	1.87E+02
6.99E+01	2.23E−02	1.33E+01	3.42E−03	2.21E−02	1.30E+01	7.60E+01
U_g = 1.41 cm/s						
5.22E−01	9.59E−04	4.18E+00	4.13E−04	9.38E−04	4.00E+00	9.50E+01
1.78E+00	5.64E−02	3.01E+00	7.88E−01	5.64E−02	3.00E+00	1.84E+00
3.27E−01	4.29E−02	6.52E+00	2.11E−01	4.11E−02	6.00E+00	6.56E+00
U_g = 2.12 cm/s						
9.05E+00	2.70E−02	1.16E+00	9.87E−01	2.51E−02	1.00E+00	1.20E+01
5.00E−02	7.17E−01	1.83E+01	7.20E−04	7.10E−01	1.80E+01	2.80E−01
1.54E+01	1.60E−01	4.30E+00	1.24E−02	1.54E−01	4.00E+00	1.63E+01

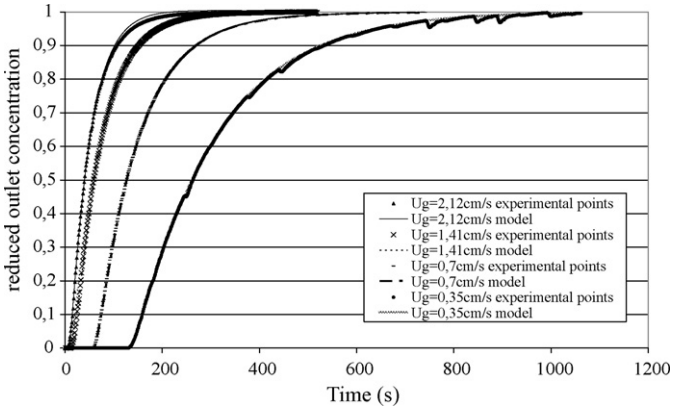

Fig. 6. Comparison between experimental and modeling points.

In the case of gas velocity being equal to 0.35 cm/s, the experimental points revealed some slope modifications. The results are illustrated in Fig. 5. This phenomenon shows the model limit in particular for the model application, it is not possible to represent a negative slope in the pulse response. For representing these experimental points, the model needs some branch in recirculation. So, it is necessary to complete the network (cf. Fig. 1), but to simply the model, we propose not to change the model. Moreover, this new branch would change the solving of the differential equation because it is necessary to add to mass balances equation so the problem became an algebra-differential system. This physical observed phenomenon in an inverse fluidized bed allows the increasing of the mass transfer. In the top of the TPIFB, the bubble stay during a long time, so the reactor became a mixed reactor. This hydrodynamics conditions present several advantages to use this reactor, in particular to have a high mass transfer and a weak abrasion.

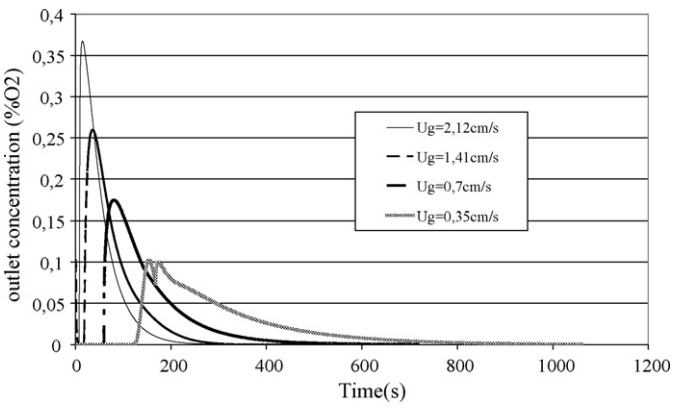

Fig. 7. Modeling Dirac pulse response with different flowrate.

In Table 5, the different volume is determined for each type of reactor. So, when the gas velocity decreases, the inverse fluidized bed became more and more a plug flow reactor. But, it is important to note that the dead volume is near to zero. When the gas flowrate increases the reactor hydrodynamics become a perfect mixing reactor.

With the value obtained in Table 6, the Dirac impulse response was modeled. In Fig. 7, the response directly read in analyzer apparatus was modeled. So, this response shows that the Dirac pulse experiments are impossible due to the gas analyzer apparatus in particular a very good calibration. When the Dirac pulse is used, it is very important to have the same signal in the section.

5. Conclusion and perspectives

A modeling technique intended for RTD simulations is proposed. The technique includes, the following reactor is presented as a reactor network involving a combination of zones representing basic ideal flow patterns (perfect mixed flow (PMF) and plug flow (PF)). The approach is based on the Mellin-modification of the Laplace transformation over the relevant equation that allows zero-time solutions for identification analysis.

The technique is applied of TPIFB. The gas and liquid phase RTDs were simulated. It is found that the increasing of the gas flowrate causes a trend of gas behavior to back mixed flow regimes. A gas velocity fall causes the inversed fluidized bed to perform largely in plug flow. The liquid phase was found to perform closer to the dispersed plug flow regime.

Appendix A

Mellin transformation of the $f(t)$ function is follow:

$$M(f(t), s) = \frac{\int_0^\infty t^{s-1} f(t)\,dt}{\Gamma(s)}$$

With s the Mellin variable (real or complex).

The different parameters were determined in the aim to obtain the Eq. (A):

$$H(p) = \frac{k\,e^{-Tp}}{(a+p)^n} \cong H'(p) = \frac{k'\,e^{-T'p}}{(a'+p)^{n'}} \quad (A)$$

with $T = T' + T''$.

The Eq. (A) was transformed into

$$G(p) = \frac{ke^{-T''p}}{(a+p)^n} \cong G'(p) = \frac{k'}{(a'+p)^{n'}} \quad (B)$$

Each function $G(p)$ and $G'(p)$ was studied in the Mellin domain.

A.1. Mellin transform of $G'(p)$

In this domain, the inverse Laplace transform was

$$g'(t) = \frac{k'}{\Gamma(n')} t^{n'-1} e^{-a't} \quad (C)$$

The Mellin transform of $g'(t)$ was

$$M(g'(t), s) = \frac{k'}{\Gamma(n')\Gamma(s)} \int_0^\infty t^{s-1} e^{-a't}\,dt \quad (D)$$

$$M(g'(t), s) = \frac{k'}{a'^{s+n'-1}} \frac{\Gamma(s+n'-1)}{\Gamma(n')\Gamma(s)} \quad (E)$$

with $\mathrm{Re}(s) > 1-\alpha$ et $\tau > 0$.

Same the method was employed for the $G(p)$ function.

A.2. Mellin transform of $G(p)$

In this domain, the inverse Laplace transform was

$$g(t) = \frac{k}{\Gamma(n)} t^{n-1} \exp(-a(t-T'')) \quad (F)$$

The Mellin transform of $g(t)$ was

$$M(h(t), s) = \frac{k}{\Gamma(n)\Gamma(s)} \int_0^\infty t^{s-1} e^{-a(t-T'')}\,dt \quad (G)$$

$$M(h, s) = \frac{ke^{a\,T''}}{a^{s+n-1}} \frac{\Gamma(s+n-1, a\,T'')}{\Gamma(n)} \quad (H)$$

With the incomplete gamma function (I):

$$\Gamma(u, x) = \int_x^\infty e^{-t} t^{u-1}\,dt = x^{u-1}e^{-x} + (u-1)\Gamma(u-1, x) \quad (I)$$

The equality of the Mellin equation $M(g(t),s)$ and $M(g'(t),s)$ allows to determine the $G(p)$ parameter versus to the $G'(p)$ parameter. For $s = 1, 2, 3$ the following relations could be determined:

$$\frac{k'}{a'^{n'}} = \frac{k}{a^n} \quad (J)$$

$$\frac{n'}{a'} = \frac{n}{a} + T'' \quad (K)$$

$$\frac{n'}{a'^2} = \frac{n}{a^2} \quad (L)$$

In case of s was superior to 3, the equality between $M(g(t),s)$ and $M(g'(t),s)$ could not deduce some relation between the different parameter.

References

[1] T. Renganathan, K. Krishnaiah, Voidage characteristics and prediction of bed expansion in liquid–solid inverse fluidized bed, Chemical Engineering Science 60 (2005) 2545–2555.

[2] I. Nikov, V. Nikolov, D. Dimitrov, Biodegradation of aniline using light carriers with optimised surface in TPIFB, Bioprocess Engineering 21 (1999) 547–552.

[3] I. Nikov, D. Karamanev, Liquid–solid mass transfer in inverse fluidized bed, AIChE Journal 37 (1991) 781–784.

[4] P. Buffiere, C. Fonade, R. Moletta, Liquid mixing and phase hold-ups in gas producing fluidized bed bioreactors, Chemical Engineering Science 53 (1998) 617–627.

[5] P. Buffiere, R. Moletta, Some hydrodynamic characteristics of inverse three phase fluidized-bed reactors, Chemical Engineering Science 54 (1999) 1233–1242.

[6] S. Michaud, N. Bernet, M. Roustan, J.P. Delgenès, Influence of hydrodynamic conditions on biofilm behavior in a methanogenic inverse turbulent bed reactor, Biotechnology Progress 19 (2003) 858–863.

[7] S. Talvy, A. Cockx, A. Line, Global modelling of a gas–liquid–solid airlift reactor, Chemical Engineering Science 60 (2005) 5991–6003.

[8] D. Dimitrov, J.-S. Guez, P. Jacques, I. Nikov, Characterization of mass tranfer in the three-phase inverse fluidized bed (TPIFB), Bulgarian Chemical Communications 36 (2004) 177–181.

[9] D. Pinelli, F. Magelli, Analysis of the fluid dynamic behavior of the liquid and gas phases in reactors stirred with multiple hydrofoil impellers, Industrial and Engineering Chemistry Research 39 (2000) 3202–3211.

[10] C. Laquerbe, J.C. Laborde, S. Soares, L. Ricciardi, P. Floquet, L. Pibouleau, S. Domenech, Computer aided synthesis of RTD models to simulate the air flow distribution in ventilated rooms, Chemical Engineering Science 56 (2001) 5727–5738.

[11] L. Montastruc, C. Azzaro-Pantel, L. Pibouleau, S. Domenech, A systemic approach for pellet reactor modeling: Application to water treatment, AIChE Journal 50 (2004) 2514–2525.

[12] A.H. Essadki, I. Nikov, H. Delmas, Local shear and skin friction on particles in three-phase fluidized beds, Chemical Engineering Science 60 (2005) 6034–6042.